

Article

Structural Insights into Plasticity and Discovery of Flavonoid Allosteric Inhibitors of Flavivirus NS2B–NS3 Protease

Marielena Vogel Saivish ^{1,2,†} , Gabriela de Lima Menezes ^{3,†} , Vivaldo Gomes da Costa ⁴ , Liliane Nebo ³ ,
Gislaine Celestino Dutra da Silva ¹ , Carolina Colombelli Pacca ^{4,5} , Rafael Elias Marques ² ,
Maurício Lacerda Nogueira ¹  and Roosevelt Alves Da Silva ^{3,*} 

¹ Departamento de Doenças Dermatológicas, Infeciosas e Parasitárias, Faculdade de Medicina de São José do Rio Preto (FAMERP), São José do Rio Preto 15090-000, Brazil

² Laboratório Nacional de Biociências, Centro Nacional de Pesquisa em Energia e Materiais (CNPEM), Campinas 13083-100, Brazil

³ Núcleo Colaborativo de Biosistemas, Universidade Federal de Jataí, Jataí 75801-615, Brazil

⁴ Instituto de Biociências, Letras e Ciências Exatas, Universidade Estadual Paulista (UNESP), São José do Rio Preto 15054-000, Brazil

⁵ Instituto Superior de Educação Ceres, Faculdade Faceres, São José do Rio Preto 15090-000, Brazil

* Correspondence: rooseveltphysicaufg@gmail.com

† These authors contributed equally to this work.

Abstract: Flaviviruses are among the most critical pathogens in tropical regions; they cause various severe diseases in developing countries but are not restricted to these countries. The development of antiviral therapeutics is crucial for managing flavivirus outbreaks. Ten proteins are encoded in the flavivirus RNA. The NS2B–NS3pro protein complex plays a fundamental role in flavivirus replication and is a promising drug target; however, no flavivirus protease inhibitors have progressed to the preclinical stage. This study analyzed the structural models and plasticity of the NS2B–NS3pro protein complex of five medically important non-dengue flaviviruses (West Nile, Rocio, Ilhéus, yellow fever, and Saint Louis encephalitis). The flavonoids amentoflavone, tetrahydrorobustaflavone, and quercetin were selected for their exceptional binding energies as potential inhibitors of the NS2B–NS3pro protein complex. AutoDock Vina results ranged from -7.0 kcal/mol to -11.5 kcal/mol and the compounds preferentially acted non-competitively. Additionally, the first structural model for the NS2B–NS3pro protein complex was proposed for Ilhéus and Rocio viruses. The NS2B–NS3pro protease is an attractive molecular target for drug development. The three identified natural flavonoids showed great inhibitory potential against the viral species. Nevertheless, further in silico and in vitro studies are required to obtain more information regarding NS2B–NS3pro inhibition by these flavonoids and their therapeutic potential.

Keywords: flaviviral protease inhibitors; Rocio virus; Ilhéus virus; Saint Louis encephalitis virus; yellow fever virus; 3D pharmacophores



Citation: Saivish, M.V.; Menezes, G.d.L.; Costa, V.G.d.; Nebo, L.; Silva, G.C.D.d.; Pacca, C.C.; Marques, R.E.; Nogueira, M.L.; Da Silva, R.A. Structural Insights into Plasticity and Discovery of Flavonoid Allosteric Inhibitors of Flavivirus NS2B–NS3 Protease. *Biophysica* **2023**, *3*, 71–92. <https://doi.org/10.3390/biophysica3010006>

Academic Editor: Paulino Gómez-Puertas

Received: 29 December 2022

Revised: 26 January 2023

Accepted: 28 January 2023

Published: 1 February 2023



Copyright: © 2023 by the authors. Licensee MDPI, Basel, Switzerland. This article is an open access article distributed under the terms and conditions of the Creative Commons Attribution (CC BY) license (<https://creativecommons.org/licenses/by/4.0/>).

1. Introduction

Flaviviruses are globally known viruses and several members of the genus (Flaviviridae family) are agents of serious diseases in humans and animals [1]. Flaviviruses have a 10–11 kb positive-sense RNA genome, which is translated into a polyprotein that is further processed by viral and host proteases to generate three structural proteins, capsid (C), pre-membrane/membrane (prM/M), and envelope (E) proteins, and at least seven non-structural (NS) proteins, NS1, NS2A, NS2B, NS3, NS4A, NS4B, and NS5 [2,3]. The 69 kDa NS3 protein is the second largest viral protein and plays several essential roles in the viral life cycle [4]. The N-terminal domain of the NS3 protein (aa 1–169) is a chymotrypsin-type serine protease (an enzyme that cleaves peptide bonds composed of three polypeptide chains linked together by disulfide bonds) that performs in cis and in trans cleavage of the

viral polyprotein [5,6]. To function properly as an active enzyme, the NS3 protease requires the NS2B cofactor [7–9]. NS2B is a 14 kDa integral membrane protein containing three domains, two transmembrane segments in the N- and C-terminal regions and a central 47-amino acid region (amino acids 49–96), which functions as an essential cofactor of NS3 protease proteins [10]. The NS3 protein of flaviviruses is neither soluble nor catalytically active as a protease *in vitro*; this suggests that it does not fold properly without the NS2B protein [11–13]. Protease activity *in vitro* was only realized after creating a soluble chimeric protein containing the hydrophilic NS2B region (residues 49–95) connected to the NS3 protease domain through a nine-amino acid linker. Host endoplasmic reticulum-derived proteases and the NS2B–NS3pro viral protease complex specifically cleave polyprotein precursors to release individual viral proteins. The C-terminal region of NS3 is an NTPase (nucleoside triphosphatase) containing a 5' terminal RNA triphosphatase (RTPase) and an RNA helicase domain. In the context of antivirals, the NS2B–NS3pro complex is described as a promising molecular target for the development of drugs against emerging flaviviruses. However, there is limited knowledge about this protein complex in the less studied and endemic flaviviruses in tropical countries.

Rocio virus (ROCV) is the etiological agent of a potentially fatal neurological infection affecting humans in Brazil. It was responsible for outbreaks resulting in the largest meningoencephalitis epidemic in the country, with over 1000 reported cases, a 13% fatality rate, and the development of permanent severe neurological sequelae in 20% of survivors [14]. This virus was last detected recently and unreported cases have been identified in the population [15]. Recently, *in silico* drug repurposing using different viral proteins identified simeprevir, daclatasvir, iloprost, and itraconazole as potential viral inhibitors [16]. Similar characteristics were observed for Ilhéus virus (ILHV), an arbovirus that caused the death of a male patient in 2017 by affecting the central nervous system [17]. Saint Louis encephalitis virus (SLEV) is another neurotropic flavivirus that poses a threat to human health in Brazil and countries with efficient health systems such as the USA [18,19]. However, no study to date has proposed *in silico* or *in vitro* antiviral agents involving the NS2B–NS3pro protein complex for ILHV or SLEV, underscoring the novelty and importance of the present work. Although yellow fever virus (YFV) has an available vaccine for humans, there are few studies related to the search for antivirals with a specific target for the NS2B–NS3pro protein complex. Most recently, *in silico* models proposed dantrolene, belinostat, olsalazine, and linezolid as possible selective inhibitors of the protein complex [20]. Most virtual *in silico* screening studies for potential agents are based on models of dengue, West Nile virus (WNV), or Zika virus (ZIKV), as they are more noticeable [21–24].

Molecular dynamics (MD) simulations can serve as powerful tools for facilitating the early phases of modern drug discovery and development processes. These simulations can obtain multiple target conformations and have been widely used in molecular docking to consider the flexibility of the targets [25,26]. Simulation techniques have become invaluable tools for modern research because they complement experimental approaches [25–28] and promising results have been observed for several different targets [22,29–32].

Currently, NS3 protease inhibitors are designed to compete with substrate binding or disrupt the interaction between NS2B and the NS3 protease domain [33–37]. There is a wealth of structural and biochemical information available on the NS2B–NS3pro substrate-binding pocket; however, no compound has progressed to the preclinical stage. This study analyzed the structural models and plasticity of the NS2B–NS3pro protein complex of five non-dengue medically important flaviviruses (WNV, ROCV, ILHV, YFV, and SLEV) and proposed the first structural models of the NS2B–NS3pro protein complexes for ILHV and ROCV. In addition, flavonoids with antiviral activity previously reported for dengue virus (DENV-2) were selected as inhibitors of these viral protein complexes.

2. Materials and Methods

The NS2B–NS3pro structures of WNV, DENV, and YFV were obtained from the Protein Data Bank (PDB ID: 2YOL [38], 3U1I [39], and 6URV [40], respectively). The NS2B–NS3pro proteins of SLEV, ROCV, and ILHV were modeled using the Robetta server by comparative modeling if they did not have a structure deposited in the PDB using the amino acid sequences from GenBank (Table 1).

Table 1. GenBank accession codes.

Virus	GenBank Accession Code
ROCV	gb:AY632542
ILHV	gb:MH932545
SLEV	gb:KM267635

ROCV: Rocio virus; ILHV: Ilhéus virus; SLEV: Saint Louis encephalitis virus.

The quality of the output models was verified using the MolProbity server [41]. The resulting models were similar to those of the WNV crystal, with only residues from the hydrophilic region considered for protein structure modeling. Histidine protonation at pH 7.4 was performed on the PropKa server [42] to simulate the protein state at physiological pH.

The MD simulation was performed using GROMACS 5.1.2 [43] software in the AMBER ff99SB-ILDN force field. The system was neutralized with Na⁺ ions, a cubic box was created 10 Å away from any protein atom to avoid interference from protein periodic image interactions, and TIP3P-type water was added. The number of Na⁺ ions and TIP3P water molecules can be seen in Table 2.

Table 2. Number of molecules added to solvate and neutralize the system.

Virus	Water Molecules	Na ⁺ Ions
ROCV	54,186	6
ILHV	49,953	1
SLEV	45,303	4

The LINCS and SETTLE algorithms [44,45] were used to constrain hydrogen and water bonds, respectively. The system temperature was adjusted to 310 K using the V-rescale algorithm (also known as the modified Berendsen algorithm) and a compressibility of 4.5×10^{-5} to simulate the physiological environment [46]. The system pressure was set to 1 bar using the Parrinello–Rahman algorithm [47]. The particle mesh Ewald (PME) summation method was used to calculate long-range electrostatic interactions and non-bonded interactions using a 1.0 nm cutoff.

The system was subjected to two steps of energy minimization (EM). These procedures aimed to ensure that the system did not have a steric clash or inappropriate geometry. Thus, the first EM was performed before solvent addition (vacuum) using two convergence criteria: the simulation would stop if the EM reached 1000 steps or if the maximum force applied to any atom was below 500 kJ/mol/nm. The second EM was performed after solvent and ion addition, the criteria were changed to 5000 steps, or the maximum force applied to any atom was below 250 kJ/mol/nm. Both EMs used the steepest descent minimization algorithm.

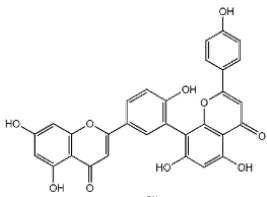
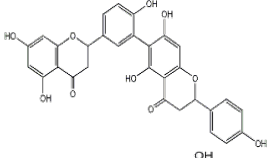
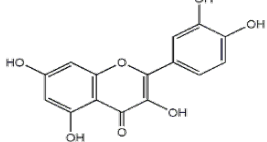
The system was then subjected to the equilibration step consisting of two 100 ps simulations, NVT ensemble and NPT ensemble, for thermodynamic equilibration with protein position restraint. Another NPT ensemble of 1 ns without protein position restraint was performed before the MD production run. The MD production run was carried out at 310 K and 150 ns without protein conformation restraint. All of these steps used the leapfrog algorithm to perform motion equation integration with a 0.2 fs time step.

Molecular dynamics trajectory analysis was performed by the root mean square deviation (RMSD) calculation using the first frame of each simulation as a reference. The

g_cluster package from GROMACS was used for cluster analysis. A cutoff of 0.25 nm was defined to perform the analysis based on the GROMOS algorithm to distinguish the conformational groups based on the RMSD profile. The GROMOS algorithm counts the number of neighbors in this defined cutoff, takes the structure with the largest number of clusters, and eliminates it from the pool of clusters. The structures representing the most present clusters throughout the simulation were chosen for molecular docking to evaluate ligand affinity in the most stable structures. The UCSF Chimera software [48] was used to visualize 3D protein behavior through all trajectories. This MD protocol was successfully applied in other studies [29–31,49,50].

The structures of quercetin, amentoflavone, and tetrahydrorobustaflavone were obtained from the PubChem website in SDF format. A summary of this information is provided in Table 3. OpenBabel software [51] converted the files to pdbqt with the addition of hydrogen at pH 7.4. Molecular docking was performed using AutoDock Vina (referred to as “Vina” in this work). The docking sites used for the analysis of all viral protein complexes were the protein active and the allosteric site defined by Sousa et al. (2015) [52]. This study tested flavonoid inhibitors that were predicted to bind in this non-competitive binding site of NS2B–NS3pro from DENV2 and DENV3.

Table 3. Information summary of flavonoid compounds.

Name	Structure	Formula	Molecular Weight
Amentoflavone		C ₃₀ H ₁₈ O ₁₀	538.0899968
Tetrahydrorobustaflavone		C ₃₀ H ₂₂ O ₁₀	542.12129692
Quercetin		C ₁₅ H ₁₀ O ₇	302.04265268

A box was defined using MGLTools to wrap the sites. One hundred docking simulations for each compound were performed for each conformation of NS2B–NS3pro to increase sampling efficiency. Each simulation generated 9 binding modes, totaling 900 modes per compound/structure. An in-house Python script was designed to define the main residues in protein–ligand interactions. The interaction cutoff was settled at 3.5 Å. The interaction type was analyzed for the best binding mode for each protein–ligand complex using the Discovery Studio Visualizer [53]. For sequence and structure comparison, the BLAST and TM-score servers were used [54,55]. Statistical comparisons of the compounds were performed using RStudio 3.6 software [56] with the Kruskal–Wallis and Wilcoxon tests.

3. Results

A crystal model of the WNV protein NS2B–NS3pro, available online in the Protein Data Bank (PDB) and identified by ID:2YOL.pdb, was selected for docking analysis. The structure of NS2B–NS3pro of DENV-3 was obtained from a crystal deposited in the Protein Data Bank (PDB ID:3U1I) containing an inhibitor (Bz-nKRR-H) linked to the active site, and the structure selected for YFV was the NS2B–NS3pro, which was retrieved from the

same database (PDB ID: 6URV). A cutoff point of 0.25 nm was selected to include the main structures during the cluster analysis simulations (Figure 1). Only one conformational group (cluster) was observed after performing MD in the ROCV NS2B–NS3pro cluster analysis (Figure 1A). This reflects the high protein stability in solution. The formation of two main conformational groups (Clusters 1 and 2) was observed for the SLEV NS2B–NS3pro protein (Figure 1B). Cluster analysis of the MD of the ILHV NS2B–NS3pro showed that Cluster 2 was more common at the beginning of the simulation until the midpoint. Cluster 1 appeared at the midpoint and remained almost exclusively until the end of the simulation (Figure 1C). Note that NS2B–NS3pro exhibited different stabilities in different species. Proteins from ROCV were more stable and those from ILHV were less stable. This was observed in the number of clusters produced (y-axis) based on the same cutoff. These stability differences between species were observed in other NS1 proteins from flaviviruses and seem to be related to amino acid sequence differences [29]. The details of the RMSD analysis are presented in Figure S1.

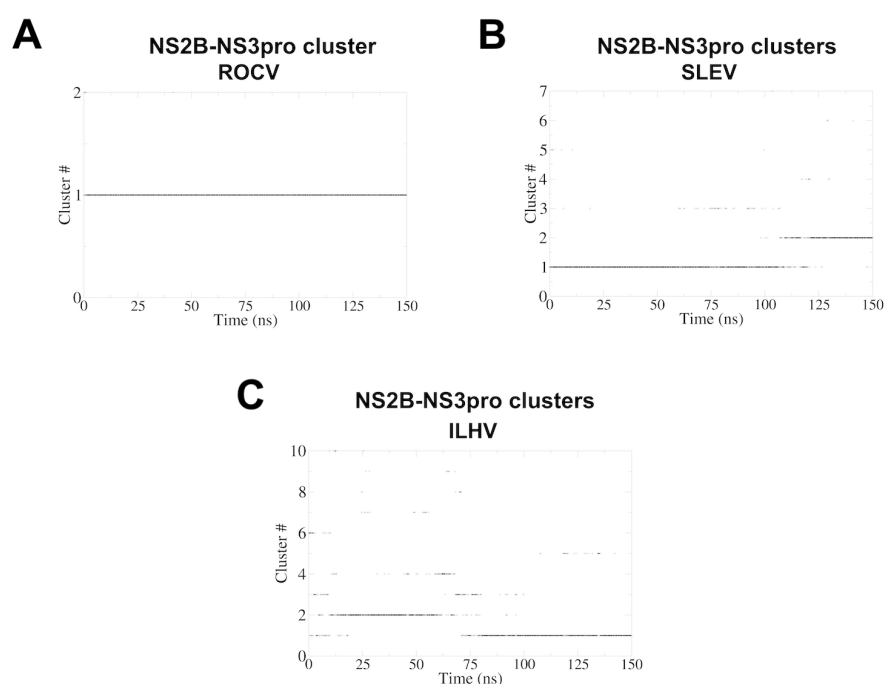


Figure 1. Cluster analysis with 0.25 nm cutoff. (A) Rocio virus, (B) Saint Louis encephalitis, (C) Ilhéus virus.

The green and blue ribbons of the cluster structures represent NS2B and NS3pro, respectively (Figure 2). Only the central structure of Cluster 1 was selected for docking analysis of ROCV and SLEV (Figure 2A,B). The proteins represented by Cluster 1 were mostly in all trajectories for both species. ILHV docking involved the two main central structures of the two clusters because Cluster 1 was not as stable as those found in ROCV and SLEV (see Figure 2C). This is important to avoid eliminating structures that appear along the trajectory and consider protein flexibility. The main differences are based on the NS2B domain because it is more flexible than NS3pro.

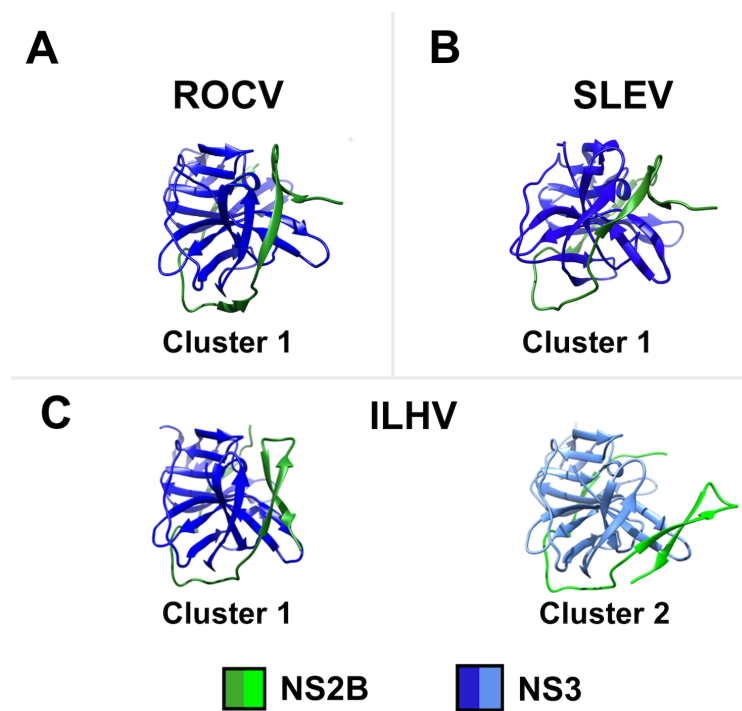


Figure 2. Ribbon conformation of clusters of (A) Rocio virus, (B) Saint Louis encephalitis, (C) Ilhéus virus. The NS2B and NS3pro domains are shown in green and blue, respectively.

The structures were deemed to be high-quality protein models since the residues in the allowed region were >98.5% according to the Ramachandran analysis and Clashscore metrics from the MolProbity server. Table 4 shows the Ramachandran analysis and Clashscore metrics. The lowest value was for the ROCV NS2B–NS3pro, where only three outliers were observed. To the best of our knowledge, these are the first structural models of this protein complex for ROCV, SLEV, and ILHV.

Table 4. Model quality analysis from MolProbity server.

Species (Cluster)	Residues in Favored Region	Residues in Allowed Region	Clashscore [†] (Percentile) [‡]
ROCV	90.9%	98.5%	2.69 (98th)
SLEV	93%	99%	3.32 (97th)
ILHV (1)	92.35%	99.5%	1.33 (99th)
ILHV (2)	95%	100%	4.66 (95th)

[†] Clashscore is the number of serious steric overlaps (>0.4 Å) per 1000 atoms. [‡] 100th: the value closest to this percentile is the best-resolved structure.

One hundred docking simulations were performed for each ligand in each NS2B–NS3pro protein complex of each virus. The box delimited for the ligand conformation search is shown in Figure 3. The box comprises the allosteric and active sites of NS2B–NS3pro. Each simulation generated 9 binding modes, totaling 900 for each ligand/protein. The highest and lowest Vina scores (also designated as energy) are shown in Table 5. High Vina scores represent lower binding affinity, and lower scores represent higher binding affinity.

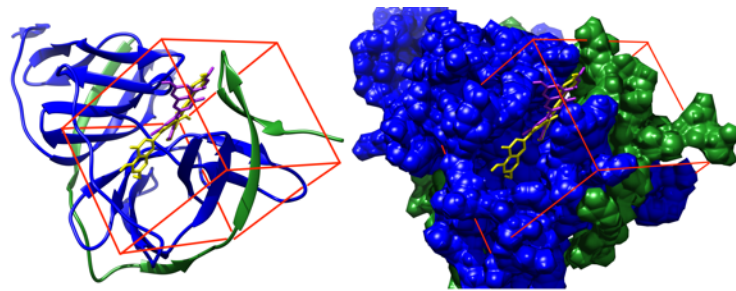


Figure 3. Delimitation of the box (grid) for the anchorage. The proteins on the left and right are on a ribbon and a surface, respectively. Yellow and lilac represent the two binding modes of amentoflavone at the allosteric site.

Table 5. Vina score (energy in kcal/mol) of each ligand after molecular docking.

Compounds	Energy	DENV-3	WNV	ROCV	SLEV	ILHV		YFV
				Cluster 1	Cluster 1	Cluster 1	Cluster 2	
Amentoflavone	Highest	−7.4	−6.9	−8.5	−7.9	−7.9	−7.4	−6.8
	Lowest	−9	−9.1	−11.5	−9.2	−9.4	−9.0	−8.8
Tetrahydrorobustaflavone	Highest	−6.7	−3.8	−7.5	−8.0	−9.3	−7.4	−2.6
	Lowest	−8	−8.6	−10.4	−9.5	−9.9	−8.3	−7.4
Quercetin	Highest	−5.8	−5.9	−7.0	−6.4	−6.8	−5.9	−6.1
	Lowest	−7.1	−8.4	−8.5	−8.9	−8.3	−7.0	−7.9

The box plot of the energy distribution of the compounds in each NS2B–NS3pro shows that amentoflavone had the lowest average in the analyses of NS2B–NS3pro for DENV3, WNV, ROCV, and YFV (Figure 4). There was no statistically significant difference in the distribution of amentoflavone and tetrahydrorobustaflavone energies in the ILHV structure (Cluster 2). Tetrahydrorobustaflavone had the lowest average energy for the NS2B–NS3pro structures of SLEV and ILHV (Cluster 1). Quercetin had the highest energy (lowest affinity) for NS2B–NS3pro in DENV3 and ROCV, whereas tetrahydrorobustaflavone had the highest energy for WNV and YFV.

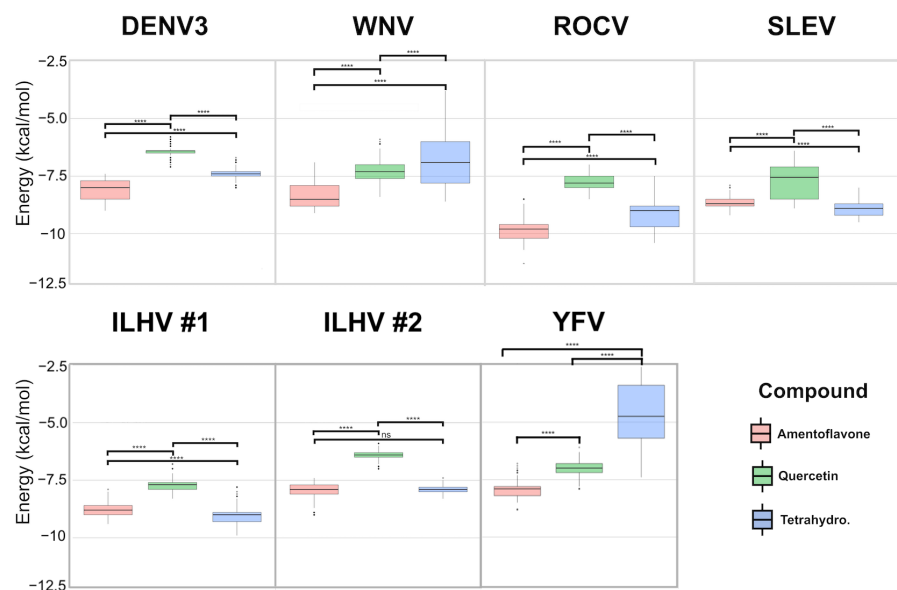


Figure 4. Box plot of the energy distributions of each ligand in dengue virus (DENV), West Nile virus (WNV), Rocio virus (ROCV), Saint Louis encephalitis virus (SLEV), Ilhéus virus (ILHV), and yellow fever virus (YFV). **** $p < 0.0001$; ns: non-significant.

The energies were lower in the conformation corresponding to Cluster 1 of ILHV for all compounds (Figure 5). This result is positive because it indicates that the ligand has a higher affinity for the most frequent structure in the simulation of this virus. Only mode 1 (lowest ligand conformation energy) was selected for each of the 100 docking runs for contact analysis. Initially, the differences between the ILHV clusters of NS2B–NS3pro were analyzed (Figure 5). Amentoflavone did not interact with any residue of the active site of the ILHV NS2B–NS3pro (51B, 75B, and 135B—His, Asp, and Ser, respectively) (Figure 5, right panel). Cluster 1 had the greatest difference in contact between clusters; more contacts were observed with residues 71A (Thr), 164B (Ala), and 165B (Ile). Meanwhile, more contacts were observed in residues 69A (Thr), 70A (Gly), 116B (Phe), 118B (Thr), 119B (Pro), 120B (Ala), 153B (Gly), and 167B (Gln) in Cluster 2. Residues 123B (Ile) and 166B (Thr) had a similar number of contacts. Note that amentoflavone had more contact with residues from Cluster 2. Amentoflavone had more contact with residues from Cluster 2. However, the type of interaction may be the determining factor in the lower energy of Cluster 1. This requires further evaluation.

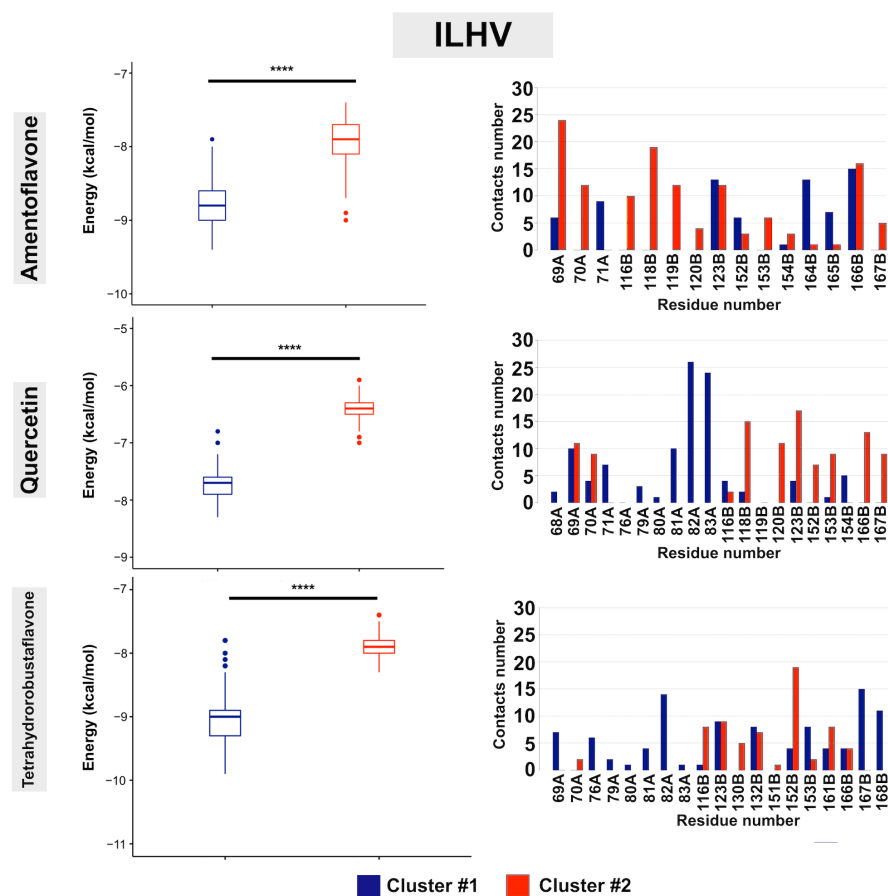


Figure 5. Comparison of energy distribution between Ilhéus (ILHV) clusters and bar graph of number of contacts per residue of NS2B and NS3pro protein complex. Chains A and B are NS2B and NS3pro, respectively. **** $p < 0.0001$.

There was a difference in the pattern of contact between different ILHV clusters for quercetin. The main contacts in Cluster 1 were with residues from the NS2B portion: 71A (Thr), 81A (Ser), 82A (Asn), and 83A (Gly). Cluster 2 had more significant contact with residues from the NS3pro portion: 118B (Thr), 120B (Ala), 123B (Ile), 152B (Asn), 153B (Gly), 166B (Thr), and 167B (Gln). Finally, analysis of the tetrahydrorobustaflavone contacts in ILHV Cluster 2 showed that the only prominent contact was with 152B (Asn). Meanwhile, Cluster 1 had contacts with 69A (Thr), 76A (Asp), 82A (Asn), 153B (Gly), 167B (Gln), and

168B (Gly). The different patterns of interaction between the NS2B–NS3pro clusters of ILHV may be related to the observed differences in structure due to protein dynamic behavior.

The number of contacts was also analyzed for the crystallographic structures and the modeled ROCV and SLEV NS2B–NS3pro complexes (Figure 6). The residues 73B (Val), 74B (Lys), 88B (Gln), 89B (Trp), and 119B (Thr) of the DENV-3 NS2B–NS3pro protein had the most contacts with amentoflavone, quercetin, and tetrahydrorobustaflavone (Figure 6A). The WNV NS2B–NS3pro protein had the most interactions with 84A (Asn), 51B (His), and 132B (Leu) (Figure 6B). Tetrahydrorobustaflavone interacted with two active site residues (51B and 135B) for the WNV protein. The ROCV NS2B–NS3pro protein complex (Figure 6C) residues that had the most interactions with amentoflavone, quercetin, and tetrahydrorobustaflavone were 75A (Leu), 30B (Thr), 80B (Ile), 124B (Lys), and 127B (Ala). The SLEV NS2B–NS3pro residues that had the most interactions were 79A (Leu), 123B (Ile), and 167B (Gln) (Figure 6D). Finally, the YFV NS2B–NS3pro residues that had the most interactions with the ligands were 91B (Gly) and 126B (Ala). These contacts are probably related to the energy differences between the ligands.

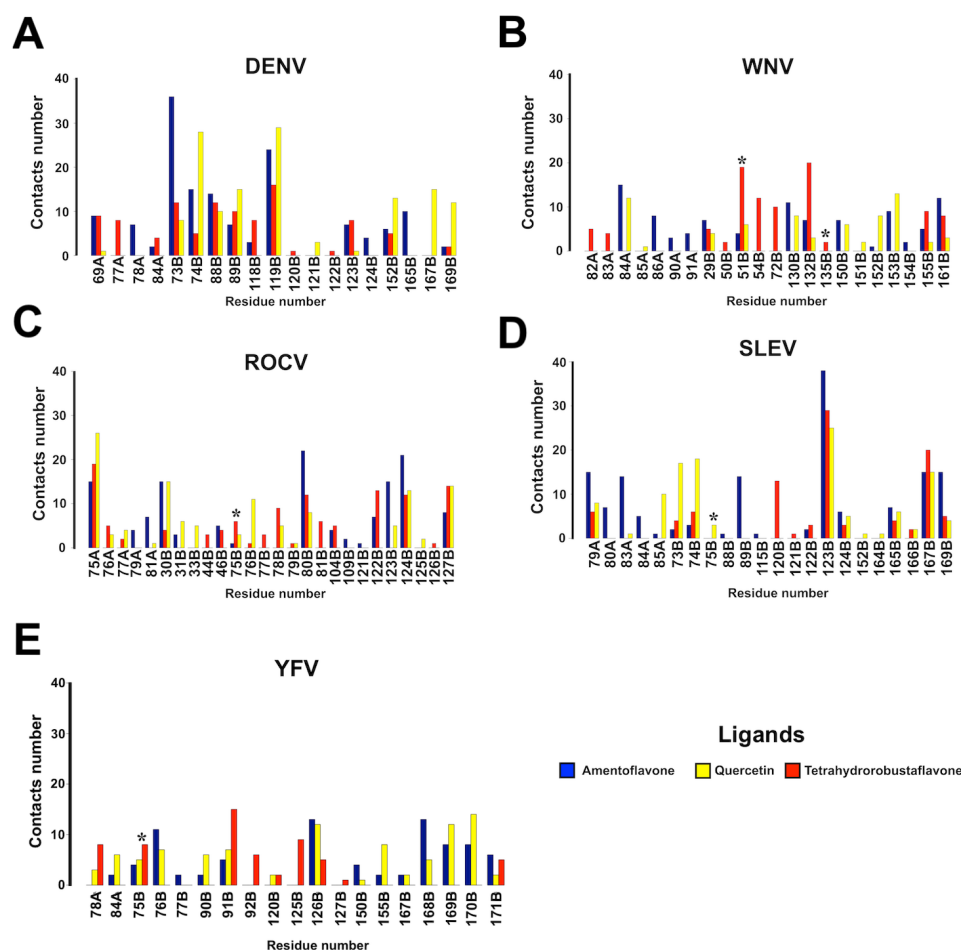


Figure 6. Bar graph of the number of contacts per residue of the NS2B–NS3pro protein complex of (A) dengue virus (DENV), (B) West Nile virus (WNV), (C) Rocio virus (ROCV), (D) Saint Louis encephalitis virus (SLEV), and (E) yellow fever virus (YFV). Chain A (NS2B) and chain B (NS3pro). * Residues from active site triad.

Separate analyses of the number of individual contacts per compound showed that the 78A (Val), 73B (Lys), and 165B (Ile) residues of DENV-3 interacted with amentoflavone (Figure 6A). Tetrahydrorobustaflavone shared many amentoflavone-like residue contacts and had unique contacts—69A (Gly), 84A (Met), 88B (Asp), 89B (Asp), 123B (Ile), 152B (Asn); these residues were also part of the allosteric site in the innermost region of the

pocket. Similarly, quercetin had contacts close to the allosteric site and in a region more external to the pocket: 74B (Lys), 89B (Trp), 119B (Thr), 152B (Asn), 167B (Gln), and 169B (Asn). This can reduce the stability of this molecule in solution because it has greater exposure to the solvent.

The lower-energy compound amentoflavone had notably greater contact with residues 84A (Asn), 130B (Tyr), and 161B (Tyr) than the other ligands after separate analysis of the number of individual contacts per compound for WNV. In addition, there were unique contacts with residues 86A (Gln), 90A (Asp), 91A (Pro), and 137B (Ser). Quercetin is an intermediate energy compound between tetrahydrorobustaflavone and amentoflavone. It had more contact with residue 153B (Gly), together with exclusive contacts with 85A (Phe) and 151B (Gly). The main difference between these residues was their location. The residues that had more contact with amentoflavone were in a more internal region of the pocket, whereas the residues with lower energy were in a region with greater exposure to the solvent. Tetrahydrorobustaflavone is a higher-energy compound that shared many contacts with each of the other ligands, allowed more interactions with residues 51B (His) and 132B (Val), and had exclusive contact with 82A (Asp), 83A (Gly), 50B (Trp), 54B (Lys), and 55B (Val). These residues were located in more internal and external locations in the pocket.

It is possible to better assess the differences between the compounds by separately analyzing the number of individual contacts per compound for ROCV (Figure 6C). This may be related to the observed differences in energy. The lower-energy compound amentoflavone had greater contact with residues 80B (Gly), 123B (Val), and 124B (Gly) than the other ligands. In addition, it exclusively made contact with residues 79A (Leu), 109B (Phe), and 103B (Gly) (Figure 6C). Quercetin is a higher-energy compound that had more contact with 75A (Leu) and 76B (Leu), in addition to exclusive contacts with 33B (Ser) and 125B (Ala). The main difference between these residues was their location. The residues that had more contact with amentoflavone were in a more internal region of the pocket, whereas the residues in contact with the lower-energy compounds were in a region with greater exposure to the solvent. Tetrahydrorobustaflavone has intermediate energy between quercetin and amentoflavone and shared many contacts with both other ligands; had more interactions with residues 75B (Asp), 78B (Thr), and 122B (Glu); and had exclusive contact with 44B (Gly), 77B (Ile), 81B (Gly), and 126B (Ile).

A separate analysis of the number of individual contacts per compound in SLEV showed that the lower-energy compound tetrahydrorobustaflavone had greater contact with 167B (Gln) than the other ligands. Furthermore, it was the only ligand to make contact with 120B (Phe) (Figure 6D). Quercetin is a higher energy compound that had more contact with 85A (Phe), 73B (Arg), 74B (Asn), together with exclusive contacts with 75B (Asp), 152B (Asn), and 164B (Gly). The main difference between these residues was their location. The residues that had more contact with tetrahydrorobustaflavone were in a region that was more internal to the pocket, whereas the residues with lower energy were in a region with greater exposure to the solvent. Amentoflavone is an intermediate energy compound between quercetin and tetrahydrorobustaflavone that shared many contacts with the other ligands at residues 79A (Leu), 123B (Ile), 124B (Gly), 165B (Ile), and 167B (Gln), together with exclusive contact with 80A (Asp), 84B (Lys), 88B (Thr), 89B (Trp), and 115B (Val).

Finally, for YFV, amentoflavone was the compound with the best binding affinity. Analysis of the contact showed that this compound had a greater number of contacts with 168B (Gln) than the other ligands (Figure 6E). It was also observed that residue 77B (Val) was in contact only with amentoflavone. Quercetin, the second-best ligand, shared many contact residues with amentoflavone (76B-Leu, 90B-Arg, 150B-Ile, 155B-Asn, 167B-Ala, 168B-Ile, 169B-Ser, and 170B-Gln). Thus, the difference in energy between these compounds and tetrahydrorobustaflavone may be related to their contacts with residues 92B (Glu) and 125B (Gly), which had only shown contacts with tetrahydrorobustaflavone, and residue 91B (Gly), which had more contact with this ligand. The stacked bar plot version of Figure 6 is shown in Figure S2.

The best and worst binding modes for each compound in the protein complex were evaluated. The allosteric site is on its left and the active site is on its right in NS2B (blue ribbon) (Figure 7). An analysis of the DENV anchors is shown in Figure 8. Amentoflavone and tetrahydrorobustaflavone only bind at the allosteric site of the DENV-3 anchors (Figure 8). This indicates that amentoflavone and tetrahydrorobustaflavone are potential non-competitive inhibitors and corroborates the findings of Sousa et al. (2015) [52].

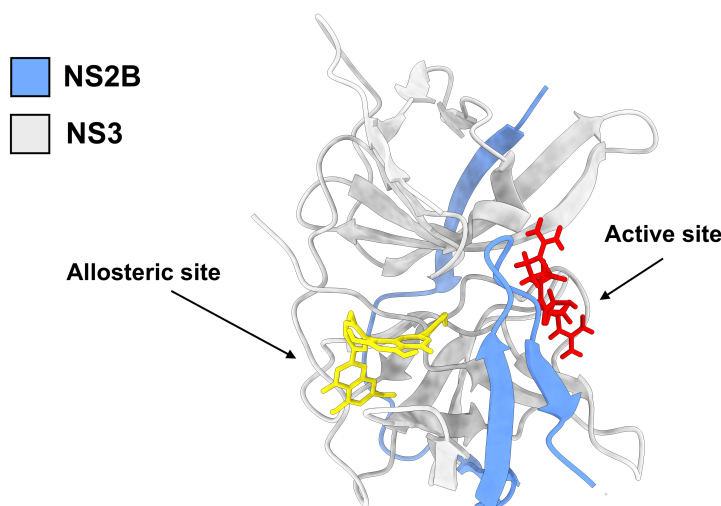


Figure 7. Representation of NS2B–NS3pro protein with emphasis on the allosteric and active sites.

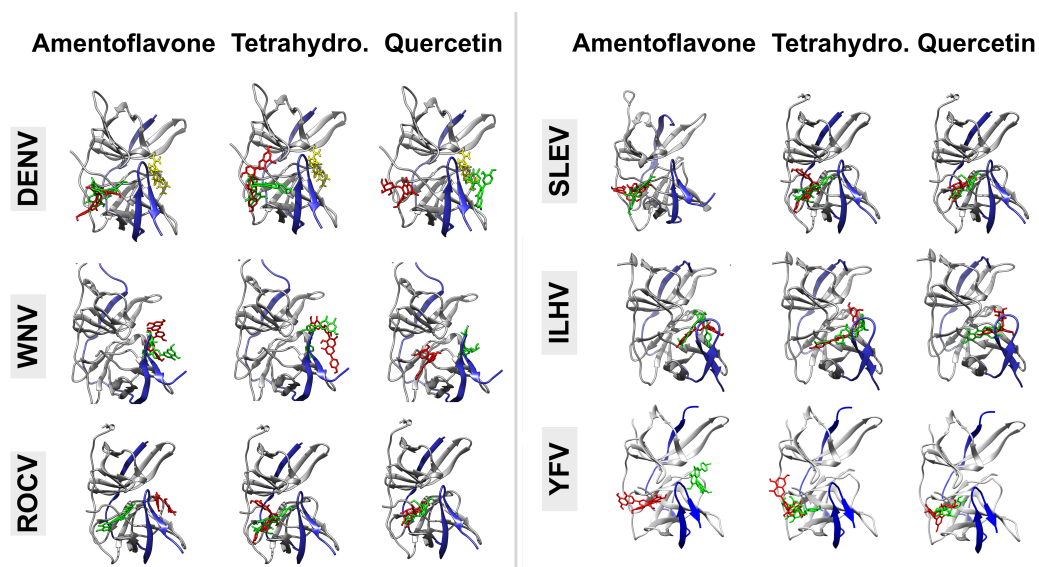


Figure 8. Representation of the binding modes of molecules in NS2B–NS3pro proteins in dengue virus (DENV), West Nile virus (WNV), Rocio virus (ROCV), Saint Louis encephalitis virus (SLEV), Ilhéus virus (ILHV), and yellow fever virus (YFV). The allosteric and active sites are on the right and left of NS2B (blue ribbon). ILHV NS2B–NS3 is only represented by Cluster 1. Cluster 2 is shown in Figure S3.

Amentoflavone and tetrahydrorobustaflavone interacted at the active site of the protein in WNV because of the larger opening of the pocket of the active site in relation to the allosteric site. Furthermore, the sizes of these molecules in the position analysis of the lowest and highest energy compounds in the ribbon structure were more amenable to binding compared with quercetin. Flavonoids preferentially bind to the allosteric site of the protein (Figure 8).

Analysis of the lowest- and highest-energy compound positions in the ribbon structure of the ROCV protein complex and the SLEV protein complex showed that quercetin and tetrahydrorobustaflavone interacted in the allosteric site of the protein. Meanwhile, the lowest-energy molecule (amentoflavone) did not bind in the active site of ROCV. This indicated that flavonoids preferentially act as non-competitive inhibitors of NS2B–NS3pro (Figure 8).

There was a difference between the binding of the higher- and lower-energy compounds in the ILHV clusters. This difference is mainly due to the change in conformation of the sites observed in the ribbon structure, favoring the binding of the active site in Cluster 1 and the allosteric site in Cluster 2. These differences can be seen in Figure 8. Taken together, these results indicate that in the Cluster 1 conformation, where binding to the active site was favored, tetrahydrorobustaflavone was the best molecule for binding. In the Cluster 2 conformation in which binding to the allosteric site was favored, there was no difference in the affinity of tetrahydrorobustaflavone and amentoflavone. Thus, both compounds are potential non-competitive inhibitors but tetrahydrorobustaflavone tends to act more as a competitive inhibitor.

In the YFV NS2B–NS3pro docking, all compounds interacted with the allosteric site of the molecule, except for the best results of amentoflavone. In this case, most of the molecules were found to be non-competitive inhibitors and, in order of energy, amentoflavone and quercetin were the most important, followed by tetrahydrorobustaflavone. The energy values observed for these ligands against the YFV NS2B–NS3pro were lower than in other studies in which the values ranged from -5.0 kcal/mol to -5.9 kcal/mol [20].

To evaluate the interacting residues and the nature of the interactions, the lower-energy binding mode of each complex was analyzed. For amentoflavone, it was observed that most of the interactions were based on van der Waals and hydrogen bonds (Figure 9). The NS2B–NS3pro proteins from WNV and YFV performed pi-pi stacking/T-shaped interactions and carbon–hydrogen bonds and hydrogen bonds with His51 from the catalytic triad. The NS2B–NS3pro protein from ILHV showed a pi-anion interaction with 75B (Asp) and a van der Waals interaction with 51B (His). Although amentoflavone was binding in the allosteric site, in the NS2B–NS3pro protein from DENV, ROCV, and SLEV, it was possible to observe a weak interaction with 75B (Asp). It appears that amentoflavone has the potential to act as both a competitive and non-competitive inhibitor, depending on the viral species.

Similar to the observations with amentoflavone, most of the interactions of tetrahydrorobustaflavone involved van der Waals interactions and hydrogen bonds (Figure 10). If we look at the residues of the catalytic triad, only the NS2B–NS3pro proteins of WNV and SLEV performed important interactions with 75B (Asp) (pi-anion type, both species) and 51B (His) (hydrogen bond and pi-pi stacked, only WNV). Therefore, for most species, this compound has better binding affinity when docked at the allosteric site.

As observed with tetrahydrorobustaflavone, the quercetin compound showed significant interactions only with the NS2B–NS3pro protein of WNV. In this case, quercetin interacted with all three residues of the catalytic triad through a pi-pi stacked interaction with 51B (His) and van der Waals interactions with 75B (Asp) and 135B (Ser) (Figure 11). Considering that both sites in Vira were subjected to the search for the best binding mode, it stands to reason that quercetin is more likely to act as a non-competitive inhibitor for most viral species, with the exception of WNV.

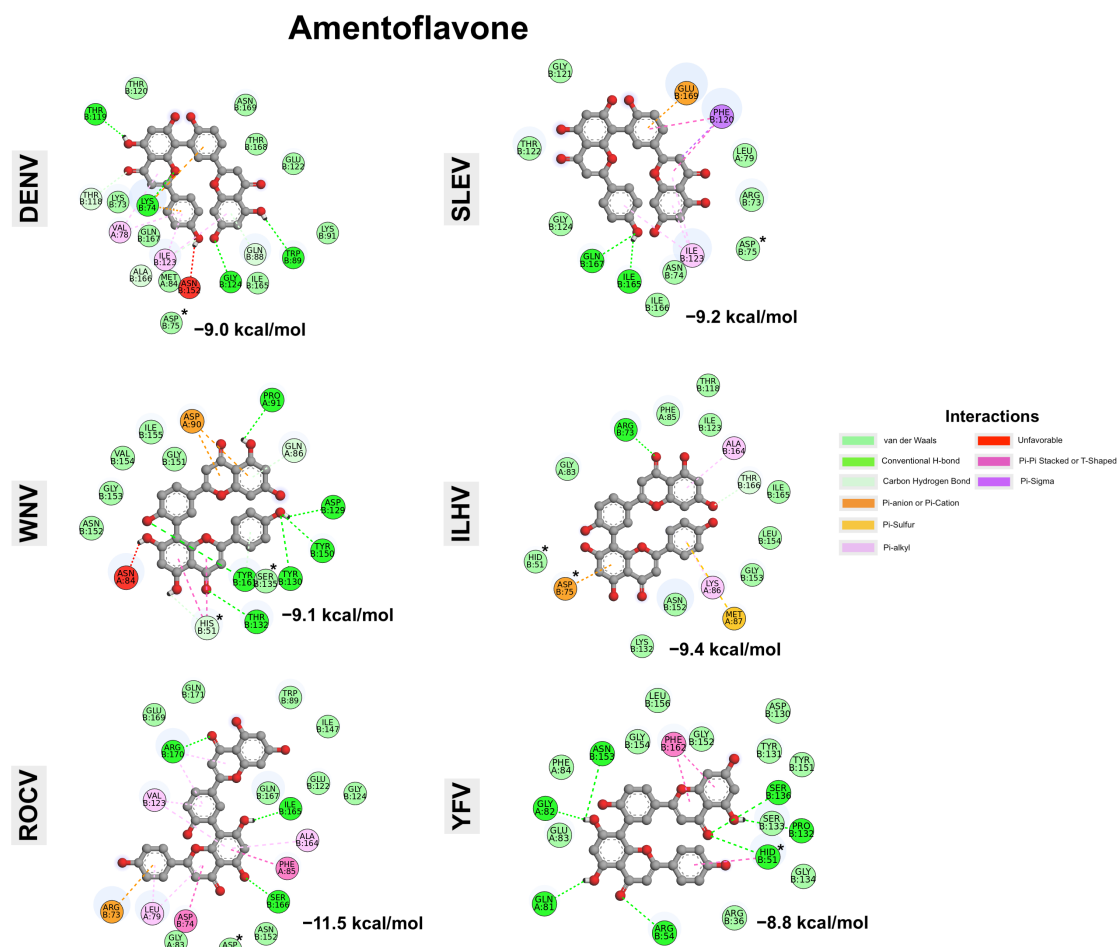


Figure 9. Interaction analysis of the best binding mode of amentoflavone in the NS2B–NS3pro proteins of dengue virus (DENV), West Nile virus (WNV), Rocio virus (ROCV), Saint Louis encephalitis virus (SLEV), Ilhéus virus (ILHV), and yellow fever virus (YFV). The residues from the catalytic triad are marked with *. ILHV NS2B–NS3pro is represented by Cluster 1 only. Cluster 2 is shown in Figure S4.

Based on the Vina scores for all the NS2B–NS3pro proteins, the ligands analyzed here showed lower values compared to the docking of chlorcyclizine (-5.6 kcal/mol) using the same protein from ZIKV. This compound showed ZIKV-induced cytopathic effects in Vero cells [22]. Our results suggest that quercetin, amentoflavone, and tetrahydrorobustaflavone have the potential to exhibit inhibitory activity against NS2B–NS3pro.

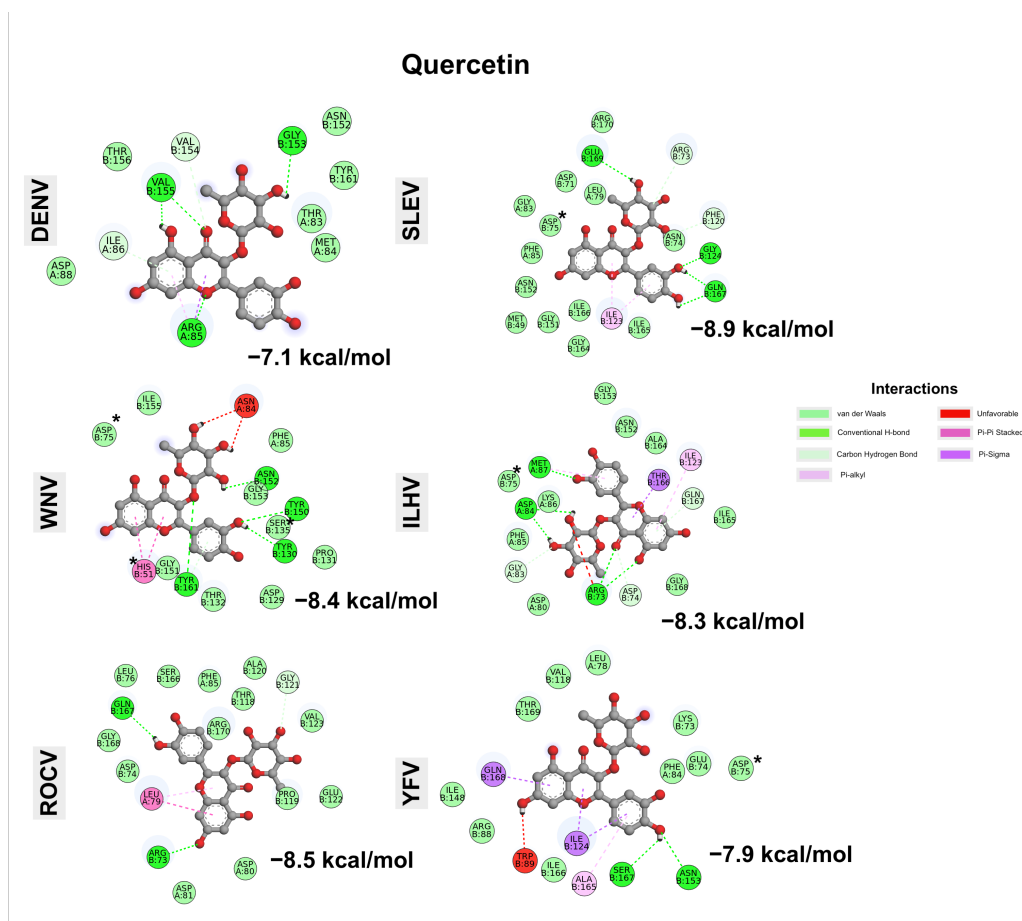


Figure 11. Interaction analysis of the best binding mode of quercetin in the NS2B–NS3pro proteins of dengue virus (DENV), West Nile virus (WNV), Rocio virus (ROCV), Saint Louis encephalitis virus (SLEV), Ilhéus virus (ILHV), and yellow fever virus (YFV). The residues from the catalytic triad are marked with *. ILHV NS2B–NS3pro is represented by Cluster 1 only. Cluster 2 is shown in Figure S4.

4. Discussion

Quercetin is ubiquitous in plant food sources and is an important bioflavonoid in the human diet. It is found in many foods and herbs and is a regular component of a normal diet. Quercetin extracts are used to treat or prevent a variety of conditions including cardiovascular disease [59], hypercholesterolemia [60], rheumatic diseases [61], infections [62–64], and cancer [65–67]. However, they were shown to be ineffective in clinical trials for several medical conditions. Quercetin is a nutritional supplement that is well tolerated and is not associated with elevated serum enzymes or episodes of clinically apparent liver injury. In addition, its therapeutic use as an antiviral has been evaluated against the influenza A (H5N1) virus [68] and its in vitro inhibitory activity against porcine epidemic diarrhea virus [69], Japanese encephalitis virus [70], dengue virus [71], Mayaro virus [72], the influenza A virus [69,73,74], animal and human herpes viruses [71,72], and the Ebola virus [75] has been described. Quercetin is an inhibitor of the NS2B–NS3pro viral enzyme including DENV [37,52,76–78]. More recently, the compound has been tested as a potential treatment for severe acute respiratory syndrome coronavirus 2 (SARS-CoV-2) infections based on several in silico studies [79–82].

Amentoflavone is a biflavonoid that is found in many natural plants. It exhibits antioxidant [83], antitumor [84], anti-inflammatory [85], neuroprotective [54], cardiovascular protective [86,87], antifungal [88], antibacterial [54], and antileishmanial activities [89,90]. Its therapeutic use as an antiviral agent has been evaluated against herpes simplex virus and human influenza [91]. Amentoflavone is an inhibitor of the viral protease enzyme [92,93].

More recently, its potential for the treatment of SARS-CoV-2 infection was proposed in several *in silico* studies [94–97].

There are limited studies of tetrahydrorobustaflavone or robustaflavone (its parent molecular structure). Robustaflavone from *Rhus succedanea* is a non-nucleoside inhibitor of hepatitis B viral replication by inhibiting RNA polymerase with an EC_{50} value of 0.25 μ M [98]. Its therapeutic use as an antiviral molecule was also evaluated against herpes simplex virus and human influenza [91]. In addition, four *in silico* studies have suggested the possible efficacy of this compound in the treatment of coronavirus disease 2019 (COVID-19) [99–102].

There are no known studies on the use of amentoflavone, tetrahydrorobustaflavone, and quercetin against YFV, ROCV, ILHV, and SLEV proteins in humans. Only quercetin has significant activity in NS2B–NS3pro inhibition for DENV. However, the present docking results suggest that amentoflavone may be an improved inhibitor candidate, as we analyzed the same serotype (DENV-3) and structure (6U1I) as Sousa et al. (2015) [52], who showed that quercetin is an excellent non-competitive DENV-2 and DENV-3 NS2B–NS3pro inhibitor.

When we compare the amino acid identity between the NS3pro of DENV-3 and the other flaviviruses (SLEV, WNV, YFV, ILHV, and ROCV) (Table 6), we can see that they have a high identity percentage and also a high TM-score value based on protein sequence and structure. Proteins with a TM-score greater than 0.5 generally adopt the same fold. Therefore, we expected that the affinity of quercetin by the NS2B–NS3pro proteins of SLEV, WNV, YFV, ILHV, and ROCV would have an affinity similar to that of the NS2B–NS3pro protein of DENV-3.

Table 6. Sequence and structure comparison of DENV and the other flaviviruses.

Virus		Identity	TM-Score
DENV-3	SLEV	60.24%	0.635
	WNV	56.63%	0.872
	YFV	55.75%	0.862
	ILHV	60.45%	0.587 */0.507 **
	ROCV	56.90%	0.790

* Result from Cluster 1. ** Result from Cluster 2.

The result of allosteric inhibition was previously studied for the ZIKV protease. It was observed that an allosteric inhibitor reduced RNA replication and protein synthesis [103]. It was also expected that flavonoids would show the same effect here since it is known that the NS2B–NS3pro protein is related to the processing of nonstructural (NS) polyproteins and that two of them, the NS1 and NS4A/NS4B proteins, support early events in viral RNA replication [104]. In summary, this study suggested that amentoflavone, tetrahydrorobustaflavone, and quercetin can be considered inhibitors of these viral species based on their exceptional binding energies. Moreover, no serious adverse events were reported for any of the selected compounds. However, few studies have assessed the safety of their use by pregnant women and people with underlying medical conditions.

5. Conclusions

The NS2B–NS3pro protease is considered an attractive molecular target for drug development because of its essential role in the flavivirus multiplication cycle. Many flaviviruses have no approved vaccine or drug; this results in millions of people developing neurological comorbidities.

Here, we performed structure-based virtual screening to investigate the antiviral activities of three natural flavonoids. Molecular docking analyses showed that amentoflavone, quercetin, and tetrahydrorobustaflavone had low binding energy (−7.0 kcal/mol to −11.5 kcal/mol). This suggested that these compounds may act against these viral species. The compounds appear to preferentially act non-competitively. Analyses of the interaction types based on multiple complexes from exhaustive docking and ligand stability in solution by molecular dynamics simulations are required. However, servers for evaluating multiple docking interac-

tions (such as nAPOLI [105] and BINANA [106]) have limitations in terms of multiple chains and the number of atoms. In addition, long computational times are required to evaluate the protein–ligand stability of six complexes in replicate. Therefore, further *in silico* and *in vitro* studies should be conducted to obtain more information on the inhibition of the NS2B–NS3pro protein and its therapeutic potential.

Supplementary Materials: The following supporting information can be downloaded at <https://www.mdpi.com/article/10.3390/biophysica3010006/s1>, Figure S1: Root mean square deviation (RMSD) analysis from molecular dynamics (MD) simulations: The RMSD evolution was different for each species. The ILHV NS2B–NS3pro (black line) is highly unstable until 80 ns, when protein becomes stable with a RMSD value of 0.3 to 0.4 nm. The Rocio virus (ROCV) NS2B–NS3pro becomes stable early than Ilhéus virus (ILHV) protein. At approximately 60 ns it is possible to see protein stability in RMSD of 0.3 nm. On the other hand, the opposite occurs for Saint Louis encephalitis virus (SLEV) NS2B–NS3pro, where protein is highly stable at the beginning of simulation (0.3 nm) but increases its RMSD values at approximately 100 ns in its trajectory; Figure S2: Stacked bar plot version of Figure 7, showing the number of contacts per residue of the NS2B–NS3pro protein complex of the dengue (DENV), West Nile (WNV), Rocio (ROCV), Saint Louis encephalitis (SLEV) and Yellow fever (YFV) viruses. In this case, it is easier to see the most contacted residues for all molecules; Figure S3: Representation of the binding modes of molecules in NS2B–NS3pro proteins from Ilhéus (ILHV). On the right of NS2B (blue ribbon) is the allosteric site and on the left is the active site; Figure S4: Interaction analysis of flavonoids and NS2B–NS3pro proteins from Ilhéus (ILHV), cluster 2.

Author Contributions: Conceptualization, G.d.L.M., M.V.S., V.G.d.C., R.A.d.S., and L.N.; methodology, G.d.L.M. and R.A.D.S.; validation, V.G.d.C., G.C.D.d.S., C.C.P., R.E.M., and M.L.N.; formal analysis, R.E.M.; investigation, G.d.L.M., M.V.S., V.G.d.C., R.A.D.S., and L.N.; writing—original draft preparation, G.d.L.M., M.V.S., V.G.d.C., and R.A.D.S.; writing—review and editing, L.N., G.C.D.d.S., C.C.P., R.E.M., and M.L.N.; supervision, R.A.D.S. All authors have read and agreed to the published version of the manuscript.

Funding: This research was funded by grant 2013/21719-3 from Fundação de Amparo à Pesquisa do Estado de São Paulo (FAPESP). M.L.N. was partially supported by the Center for Research in Emerging Infectious Disease “The Coordinating Research on Emerging Arboviral Threats Encompassing the Neotropics (CREATE-NEO)” grant U01AI151807 awarded by the National Institutes of Health (NIH, USA). M.L.N. was a Conselho Nacional de Desenvolvimento Científico e Tecnológico CNPq Research Fellow. M.V.S. was supported by FAPESP Ph.D. Scholarship Number 2020/12875-5. V.G.d.C. was funded by a postdoctoral fellowship from Universidade Estadual Paulista (UNESP), project number: 4320 (Edital PROPe 13/2022). G.d.L.M. was supported by a Coordenação de Aperfeiçoamento de Pessoal de Nível Superior (CAPES) Ph.D. scholarship.

Institutional Review Board Statement: Not applicable.

Data Availability Statement: Not applicable.

Acknowledgments: The authors wish to thank LaMCAD (the Multiuser High-Performance Computing Laboratory) at the Universidade Federal de Goiás for allowing them to use their high-performance cluster.

Conflicts of Interest: The authors declare no conflicts of interest

References

1. Pierson, T.C.; Diamond, M.S. The continued threat of emerging flaviviruses. *Nat. Microbiol.* **2020**, *5*, 796–812. [[CrossRef](#)] [[PubMed](#)]
2. Fernandez-Garcia, M.D.; Mazzon, M.; Jacobs, M.; Amara, A. Pathogenesis of Flavivirus Infections: Using and Abusing the Host Cell. *Cell Host Microbe* **2009**, *5*, 318–328. [[CrossRef](#)] [[PubMed](#)]
3. Fishburn, A.T.; Pham, O.H.; Kenaston, M.W.; Beesabathuni, N.S.; Shah, P.S. Let’s Get Physical: Flavivirus–Host Protein–Protein Interactions in Replication and Pathogenesis. *Front. Microbiol.* **2022**, *13*, 847588. [[CrossRef](#)] [[PubMed](#)]
4. Li, K.; Phoo, W.W.; Luo, D. Functional interplay among the flavivirus NS3 protease, helicase, and cofactors. *Virol. Sin.* **2014**, *29*, 74–85. [[CrossRef](#)]
5. Chambers, T.J.; Hahn, C.S.; Galler, R.; Rice, C.M. Flavivirus Genome Organization, Expression, and Replication. *Annu. Rev. Microbiol.* **1990**, *44*, 649–688. [[CrossRef](#)]

6. Li, L.; Lok, S.M.; Yu, I.M.; Zhang, Y.; Kuhn, R.J.; Chen, J.; Rossmann, M.G. The Flavivirus Precursor Membrane-Envelope Protein Complex: Structure and Maturation. *Science* **2008**, *319*, 1830–1834. [[CrossRef](#)]
7. Chappell, K.J.; Stoermer, M.J.; Fairlie, D.P.; Young, P.R. Mutagenesis of the West Nile virus NS2B cofactor domain reveals two regions essential for protease activity. *J. Gen. Virol.* **2008**, *89*, 1010–1014. [[CrossRef](#)]
8. Falgout, B.; Miller, R.; Lai, C.J. Deletion analysis of dengue virus type 4 nonstructural protein NS2B: Identification of a domain required for NS2B-NS3 protease activity. *J. Virol.* **1993**, *67*, 2034–2042. [[CrossRef](#)]
9. Niyomrattanakit, P.; Winoyanu wattikun, P.; Chanprapaph, S.; Angsuthanasombat, C.; Panyim, S.; Katzenmeier, G. Identification of Residues in the Dengue Virus Type 2 NS2B Cofactor That Are Critical for NS3 Protease Activation. *J. Virol.* **2004**, *78*, 13708–13716. [[CrossRef](#)]
10. Clum, S.; Ebner, K.E.; Padmanabhan, R. Cotranslational Membrane Insertion of the Serine Proteinase Precursor NS2B-NS3(Pro) of Dengue Virus Type 2 Is Required for Efficient *In Vitro* Processing and Is Mediated through the Hydrophobic Regions of NS2B. *J. Biol. Chem.* **1997**, *272*, 30715–30723. [[CrossRef](#)]
11. Phoo, W.W.; Sahili, A.E.; Zhang, Z.; Chen, M.W.; Liew, C.W.; Lescar, J.; Vasudevan, S.G.; Luo, D. Crystal structures of full length DENV4 NS2B-NS3 reveal the dynamic interaction between NS2B and NS3. *Antivir. Res.* **2020**, *182*, 104900. [[CrossRef](#)]
12. Tseng, A.C.; Nerurkar, V.R.; Neupane, K.R.; Kae, H.; Kaufusi, P.H. Potential Dual Role of West Nile Virus NS2B in Orchestrating NS3 Enzymatic Activity in Viral Replication. *Viruses* **2021**, *13*, 216. [[CrossRef](#)]
13. Xu, T.; Sampath, A.; Chao, A.; Wen, D.; Nanao, M.; Luo, D.; Chene, P.; Vasudevan, S.G.; Lescar, J. Towards the Design of Flavivirus Helicase/NTPase Inhibitors: Crystallographic and Mutagenesis Studies of the Dengue Virus NS3 Helicase Catalytic Domain. In *Novartis Foundation Symposia*; John Wiley & Sons, Ltd.: Hoboken, NJ, USA, 2008; pp. 87–101. [[CrossRef](#)]
14. Saivish, M.V.; da Costa, V.G.; de Lima Menezes, G.; da Silva, R.A.; da Silva, G.C.D.; Moreli, M.L.; Sacchetto, L.; Pacca, C.C.; Vasilakis, N.; Nogueira, M.L. Rocio Virus: An Updated View on an Elusive Flavivirus. *Viruses* **2021**, *13*, 2293. [[CrossRef](#)]
15. Saivish, M.V.; da Costa, V.G.; Rodrigues, R.L.; Féres, V.C.; Montoya-Diaz, E.; Moreli, M.L. Detection of Rocio Virus SPH 34675 during Dengue Epidemics, Brazil, 2011–2013. *Emerg. Infect. Dis.* **2020**, *26*, 797–799. [[CrossRef](#)]
16. Sagini, J.P.; Arantes, P.R.; Pedebos, C.; Ligabue-Braun, R. Rocio Virus Encephalitis: *In Silico* Evidence for Drug Repurposing. *Macromol* **2022**, *2*, 100–112. [[CrossRef](#)]
17. Milhim, B.H.G.A.; Estofolete, C.F.; da Rocha, L.C.; Liso, E.; Brienze, V.M.S.; Vasilakis, N.; Terzian, A.C.B.; Nogueira, M.L. Fatal Outcome of Ilheus Virus in the Cerebrospinal Fluid of a Patient Diagnosed with Encephalitis. *Viruses* **2020**, *12*, 957. [[CrossRef](#)]
18. Diaz, A.; Coffey, L.L.; Burkett-Cadena, N.; Day, J.F. Reemergence of St. Louis Encephalitis Virus in the Americas. *Emerg. Infect. Dis.* **2018**, *24*, 2150. [[CrossRef](#)]
19. Swetnam, D.M.; Stuart, J.B.; Young, K.; Maharaj, P.D.; Fang, Y.; Garcia, S.; Barker, C.M.; Smith, K.; Godsey, M.S.; Savage, H.M.; et al. Movement of St. Louis encephalitis virus in the Western United States, 2014–2018. *PLoS Neglected Trop. Dis.* **2020**, *14*, e0008343. [[CrossRef](#)]
20. Odhar, H.A.; Ahjel, S.W.; Albeer, A.A.M.A.; Hashim, A.F.; Humadi, S.S. Virtual Screening of FDA Approved Drugs Library to Identify a Potential Inhibitor against NS2B-NS3 Protease of Yellow Fever Virus. *J. Pharm. Res. Int.* **2021**, *33*, 177–186. [[CrossRef](#)]
21. Brecher, M.; Li, Z.; Liu, B.; Zhang, J.; Koetzner, C.A.; Alifarag, A.; Jones, S.A.; Lin, Q.; Kramer, L.D.; Li, H. A conformational switch high-throughput screening assay and allosteric inhibition of the flavivirus NS2B-NS3 protease. *PLoS Pathog.* **2017**, *13*, e1006411. [[CrossRef](#)]
22. Santos, F.R.S.; Nunes, D.A.F.; Lima, W.G.; Davyt, D.; Santos, L.L.; Taranto, A.G.; Ferreira, J.M.S. Identification of Zika Virus NS2B-NS3 Protease Inhibitors by Structure-Based Virtual Screening and Drug Repurposing Approaches. *J. Chem. Inf. Model.* **2019**, *60*, 731–737. [[CrossRef](#)] [[PubMed](#)]
23. Virtual Ligand Screening of the National Cancer Institute (NCI) Compound Library Leads to the Allosteric Inhibitory Scaffolds of the West Nile Virus NS3 Proteinase ASSAY and Drug Development Technologies. Available online: <https://www.liebertpub.com/doi/abs/10.1089/adt.2010.0309> (accessed on 17 April 2022).
24. Shin, H.J.; Kim, M.H.; Lee, J.Y.; Hwang, I.; Yoon, G.Y.; Kim, H.S.; Kwon, Y.C.; Ahn, D.G.; Kim, K.D.; Kim, B.T.; et al. Structure-Based Virtual Screening: Identification of a Novel NS2B-NS3 Protease Inhibitor with Potent Antiviral Activity against Zika and Dengue Viruses. *Microorganisms* **2021**, *9*, 545. [[CrossRef](#)] [[PubMed](#)]
25. Liu, X.; Shi, D.; Zhou, S.; Liu, H.; Liu, H.; Yao, X. Molecular dynamics simulations and novel drug discovery. *Expert Opin. Drug Discov.* **2017**, *13*, 23–37. [[CrossRef](#)] [[PubMed](#)]
26. Salo-Ahen, O.M.H.; Alanko, I.; Bhadane, R.; Bonvin, A.M.J.J.; Honorato, R.V.; Hossain, S.; Juffer, A.H.; Kbedev, A.; Lahtela-Kakkonen, M.; Larsen, A.S.; et al. Molecular Dynamics Simulations in Drug Discovery and Pharmaceutical Development. *Processes* **2020**, *9*, 71. [[CrossRef](#)]
27. Amaro, R.E.; Baudry, J.; Chodera, J.; Demir, O.; McCammon, J.A.; Miao, Y.; Smith, J.C. Ensemble Docking in Drug Discovery. *Biophys. J.* **2018**, *114*, 2271–2278. [[CrossRef](#)]
28. Śledź, P.; Cafilisch, A. Protein structure-based drug design: From docking to molecular dynamics. *Curr. Opin. Struct. Biol.* **2018**, *48*, 93–102. [[CrossRef](#)]
29. de Lima Menezes, G.; Saivish, M.V.; Nogueira, M.L.; da Silva, R.A. Virtual screening of small natural compounds against NS1 protein of DENV, YFV and ZIKV. *J. Biomol. Struct. Dyn.* **2022**, 1–11. [[CrossRef](#)]
30. de Lima Menezes, G.; da Silva, R.A. Identification of potential drugs against SARS-CoV-2 non-structural protein 1 (nsp1). *J. Biomol. Struct. Dyn.* **2020**, *39*, 5657–5667. [[CrossRef](#)]

31. Gonçalves, R.L.; de Lima Menezes, G.; Sussuchi, L.; Moreli, M.L.; Mottin, M.; Andrade, C.H.; Pereira, M.; da Silva, R.A. Dynamic behavior of Dengue and Zika viruses NS1 protein reveals monomer–monomer interaction mechanisms and insights to rational drug design. *J. Biomol. Struct. Dyn.* **2019**, *38*, 4353–4363. [CrossRef]
32. Santos, N.P.; Santos, L.H.; de Magalhães, M.T.Q.; Lei, J.; Hilgenfeld, R.; Ferreira, R.S.; Bleicher, L. Characterization of an Allosteric Pocket in Zika Virus NS2B-NS3 Protease. *J. Chem. Inf. Model.* **2022**, *62*, 945–957. [CrossRef]
33. Lim, S.P.; Wang, Q.Y.; Noble, C.G.; Chen, Y.L.; Dong, H.; Zou, B.; Yokokawa, F.; Nilar, S.; Smith, P.; Beer, D.; et al. Ten years of dengue drug discovery: Progress and prospects. *Antivir. Res.* **2013**, *100*, 500–519. [CrossRef]
34. Luo, D.; Vasudevan, S.G.; Lescar, J. The flavivirus NS2B–NS3 protease–helicase as a target for antiviral drug development. *Antivir. Res.* **2015**, *118*, 148–158. [CrossRef]
35. Nie, S.; Yao, Y.; Wu, F.; Wu, X.; Zhao, J.; Hua, Y.; Wu, J.; Huo, T.; Lin, Y.L.; Kneubehl, A.R.; et al. Synthesis, Structure–Activity Relationships, and Antiviral Activity of Allosteric Inhibitors of Flavivirus NS2B–NS3 Protease. *J. Med. Chem.* **2021**, *64*, 2777–2800. [CrossRef]
36. Takagi, Y.; Matsui, K.; Nobori, H.; Maeda, H.; Sato, A.; Kurosu, T.; Orba, Y.; Sawa, H.; Hattori, K.; Higashino, K.; et al. Discovery of novel cyclic peptide inhibitors of dengue virus NS2B-NS3 protease with antiviral activity. *Bioorg. Med. Chem. Lett.* **2017**, *27*, 3586–3590. [CrossRef]
37. Yao, C.; Xi, C.; Hu, K.; Gao, W.; Cai, X.; Qin, J.; Lv, S.; Du, C.; Wei, Y. Inhibition of enterovirus 71 replication and viral 3C protease by quercetin. *Viol. J.* **2018**, *15*, 116. [CrossRef]
38. Hammamy, M.Z.; Haase, C.; Hammami, M.; Hilgenfeld, R.; Steinmetzer, T. Development and Characterization of New Peptidomimetic Inhibitors of the West Nile Virus NS2B-NS3 Protease. *ChemMedChem* **2013**, *8*, 231–241. [CrossRef]
39. Noble, C.G.; Seh, C.C.; Chao, A.T.; Shi, P.Y. Ligand-Bound Structures of the Dengue Virus Protease Reveal the Active Conformation. *J. Virol.* **2012**, *86*, 438–446. [CrossRef]
40. Noske, G.D.; Gawriljuk, V.O.; Fernandes, R.S.; Furtado, N.D.; Bonaldo, M.C.; Oliva, G.; Godoy, A.S. Structural characterization and polymorphism analysis of the NS2B-NS3 protease from the 2017 Brazilian circulating strain of Yellow Fever virus. *Biochim. Biophys. Acta* **2020**, *1864*, 129521. [CrossRef]
41. Williams, C.J.; Headd, J.J.; Moriarty, N.W.; Prisant, M.G.; Videau, L.L.; Deis, L.N.; Verma, V.; Keedy, D.A.; Hintze, B.J.; Chen, V.B.; et al. MolProbity: More and better reference data for improved all-atom structure validation. *Protein Sci.* **2017**, *27*, 293–315. [CrossRef]
42. Olsson, M.H.M.; Søndergaard, C.R.; Rostkowski, M.; Jensen, J.H. PROPKA3: Consistent treatment of internal and surface residues in empirical pKa predictions. *J. Chem. Theory Comput.* **2011**, *7*, 525–537. [CrossRef]
43. Abraham, M.J.; Murtola, T.; Schulz, R.; Páll, S.; Smith, J.C.; Hess, B.; Lindahl, E. GROMACS: High performance molecular simulations through multi-level parallelism from laptops to supercomputers. *SoftwareX* **2015**, *1-2*, 19–25. [CrossRef]
44. Hess, B.; Bekker, H.; Berendsen, H.J.C.; Fraaije, J.G.E.M. LINCS: A linear constraint solver for molecular simulations. *J. Comput. Chem.* **1997**, *18*, 1463–1472. [CrossRef]
45. Miyamoto, S.; Kollman, P.A. Settle: An analytical version of the SHAKE and RATTLE algorithm for rigid water models. *J. Comput. Chem.* **1992**, *13*, 952–962. [CrossRef]
46. Berendsen, H.J.C.; Postma, J.P.M.; van Gunsteren, W.F.; DiNola, A.; Haak, J.R. Molecular dynamics with coupling to an external bath. *J. Chem. Phys.* **1984**, *81*, 3684–3690. [CrossRef]
47. Hutter, J. Car-Parrinello molecular dynamics. *WIREs Comput. Mol. Sci.* **2011**, *2*, 604–612. [CrossRef]
48. Pettersen, E.F.; Goddard, T.D.; Huang, C.C.; Couch, G.S.; Greenblatt, D.M.; Meng, E.C.; Ferrin, T.E. UCSF Chimera?A visualization system for exploratory research and analysis. *J. Comput. Chem.* **2004**, *25*, 1605–1612. [CrossRef]
49. da Silva, I.R.; Parise, M.R.; Pereira, M.; da Silva, R.A. Prospecting for new catechol-O-methyltransferase (COMT) inhibitors as a potential treatment for Parkinson’s disease: A study by molecular dynamics and structure-based virtual screening. *J. Biomol. Struct. Dyn.* **2020**, *39*, 5872–5891. [CrossRef]
50. de Oliveira, F.M.; Procopio, V.O.; de Lima Menezes, G.; da Silva, R.A.; Kipnis, A.; Junqueira-Kipnis, A.P. Mycobacterium bovis PknG R242P Mutation Results in Structural Changes with Enhanced Virulence in the Mouse Model of Infection. *Microorganisms* **2022**, *10*, 673. [CrossRef]
51. O’Boyle, N.M.; Banck, M.; James, C.A.; Morley, C.; Vandermeersch, T.; Hutchison, G.R. Open Babel: An open chemical toolbox. *J. Cheminform.* **2011**, *3*, 33. [CrossRef]
52. de Sousa, L.R.F.; Wu, H.; Nebo, L.; Fernandes, J.B.; das Graças Fernandes da Silva, M.F.; Kiefer, W.; Kanitz, M.; Bodem, J.; Diederich, W.E.; Schirmeister, T.; et al. Flavonoids as noncompetitive inhibitors of Dengue virus NS2B-NS3 protease: Inhibition kinetics and docking studies. *Bioorg. Med. Chem.* **2015**, *23*, 466–470. [CrossRef]
53. Free Download: BIOVIA Discovery Studio Visualizer [Online]. Available online: <https://discover.3ds.com/discovery-studio-visualizer-download> (accessed on 19 January 2023).
54. Zhang, Y.; Skolnick, J. Scoring function for automated assessment of protein structure template quality. *Proteins* **2004**, *57*, 702–710. [CrossRef]
55. Madden, T.; Tatusov, R.; Zhang, J. *Applications of Network BLAST Server*; Elsevier: Amsterdam, The Netherlands, 1996.
56. RStudio Team. *RStudio: Integrated Development Environment for R*; RStudio, PBC: Boston, MA, USA, 2021.
57. Noble, C.G.; Shi, P.Y. Structural biology of dengue virus enzymes: Towards rational design of therapeutics. *Antivir. Res.* **2012**, *96*, 115–126. [CrossRef]

58. Erbel, P.; Schiering, N.; D'Arcy, A.; Renatus, M.; Kroemer, M.; Lim, S.P.; Yin, Z.; Keller, T.H.; Vasudevan, S.G.; Hommel, U. Structural basis for the activation of flaviviral NS3 proteases from dengue and West Nile virus. *Nat. Struct. Mol. Biol.* **2006**, *13*, 372–373. [[CrossRef](#)]
59. Gormaz, J.; Quintremil, S.; Rodrigo, R. Cardiovascular Disease: A Target for the Pharmacological Effects of Quercetin. *CTMC* **2015**, *15*, 1735–1742. [[CrossRef](#)]
60. Mariee, A.D.; Abd-Allah, G.M.; El-Beshbishy, H.A. Protective effect of dietary flavonoid quercetin against lipemic-oxidative hepatic injury in hypercholesterolemic rats. *Pharm. Biol.* **2012**, *50*, 1019–1025. [[CrossRef](#)]
61. Javadi, F.; Ahmadzadeh, A.; Egtesadi, S.; Aryaeian, N.; Zabihiyeganeh, M.; Foroushani, A.R.; Jazayeri, S. The Effect of Quercetin on Inflammatory Factors and Clinical Symptoms in Women with Rheumatoid Arthritis: A Double-Blind, Randomized Controlled Trial. *J. Am. Coll. Nutr.* **2016**, *36*, 9–15. [[CrossRef](#)]
62. Jaisinghani, R.N. Antibacterial properties of quercetin. *Microbiol. Res.* **2017**, *8*, 6877. [[CrossRef](#)]
63. Mead, J.R.; McNair, N. Antiparasitic activity of flavonoids and isoflavones against *Cryptosporidium parvum* and *Encephalitozoon intestinalis*. *FEMS Microbiol. Lett.* **2006**, *259*, 153–157. [[CrossRef](#)]
64. Salehi, B.; Machin, L.; Monzote, L.; Sharifi-Rad, J.; Ezzat, S.M.; Salem, M.A.; Merghany, R.M.; Mahdy, N.M.E.; Kılıç, C.S.; Sytar, O.; et al. Therapeutic Potential of Quercetin: New Insights and Perspectives for Human Health. *ACS Omega* **2020**, *5*, 11849–11872. [[CrossRef](#)]
65. Ezzati, M.; Yousefi, B.; Velaei, K.; Safa, A. A review on anti-cancer properties of Quercetin in breast cancer. *Life Sci.* **2020**, *248*, 117463. [[CrossRef](#)]
66. Gibellini, L.; Pinti, M.; Nasi, M.; Montagna, J.P.; Biasi, S.D.; Roat, E.; Bertocelli, L.; Cooper, E.L.; Cossarizza, A. Quercetin and Cancer Chemoprevention. *Evid. Based Complement. Altern. Med.* **2011**, *2011*, 591356. [[CrossRef](#)] [[PubMed](#)]
67. Murakami, A.; Ashida, H.; Terao, J. Multitargeted cancer prevention by quercetin. *Cancer Lett.* **2008**, *269*, 315–325. [[CrossRef](#)] [[PubMed](#)]
68. Friel, H.; Lederman, H. A nutritional supplement formula for influenza A (H5N1) infection in humans. *Med. Hypotheses* **2006**, *67*, 578–587. [[CrossRef](#)] [[PubMed](#)]
69. Choi, H.J.; Song, J.H.; Park, K.S.; Kwon, D.H. Inhibitory effects of quercetin 3-rhamnoside on influenza A virus replication. *Eur. J. Pharm. Sci.* **2009**, *37*, 329–333. [[CrossRef](#)]
70. Johari, J.; Kianmehr, A.; Mustafa, M.; Abubakar, S.; Zandi, K. Antiviral Activity of Baicalein and Quercetin against the Japanese Encephalitis Virus. *Int. J. Mol. Sci.* **2012**, *13*, 16785–16795. [[CrossRef](#)]
71. Zandi, K.; Teoh, B.T.; Sam, S.S.; Wong, P.F.; Mustafa, M.R.; AbuBakar, S. Antiviral activity of four types of bioflavonoid against dengue virus type-2. *Viol. J.* **2011**, *8*, 1–11. [[CrossRef](#)]
72. dos Santos, A.E.; Kuster, R.M.; Yamamoto, K.A.; Salles, T.S.; Campos, R.; de Meneses, M.D.; Soares, M.R.; Ferreira, D. Quercetin and quercetin 3-O-glycosides from *Bauhinia longifolia* (Bong.) Steud. show anti-Mayaro virus activity. *Parasites Vectors* **2014**, *7*, 1–7. [[CrossRef](#)]
73. Choi, H.J.; Song, J.H.; Kwon, D.H. Quercetin 3-rhamnoside Exerts Antiinfluenza A Virus Activity in Mice. *Phytother. Res.* **2011**, *26*, 462–464. [[CrossRef](#)]
74. Wu, W.; Li, R.; Li, X.; He, J.; Jiang, S.; Liu, S.; Yang, J. Quercetin as an Antiviral Agent Inhibits Influenza A Virus (IAV) Entry. *Viruses* **2015**, *8*, 6. [[CrossRef](#)]
75. Fanunza, E.; Iampietro, M.; Distinto, S.; Corona, A.; Quartu, M.; Maccioni, E.; Horvat, B.; Tramontano, E. Quercetin Blocks Ebola Virus Infection by Counteracting the VP24 Interferon-Inhibitory Function. *Antimicrob. Agents Chemother.* **2020**, *64*, e00530-20. [[CrossRef](#)]
76. Bahun, M.; Jukić, M.; Oblak, D.; Kranjc, L.; Bajc, G.; Butala, M.; Bozovičar, K.; Bratkovič, T.; Podlipnik, Č.; Ulrih, N.P. Inhibition of the SARS-CoV-2 3CLpro main protease by plant polyphenols. *Food Chem.* **2022**, *373*, 131594. [[CrossRef](#)]
77. Li, Z.; Cao, H.; Cheng, Y.; Zhang, X.; Zeng, W.; Sun, Y.; Chen, S.; He, Q.; Han, H. Inhibition of Porcine Epidemic Diarrhea Virus Replication and Viral 3C-Like Protease by Quercetin. *Int. J. Mol. Sci.* **2020**, *21*, 8095. [[CrossRef](#)]
78. Lima, C.S.; Mottin, M.; de Assis, L.R.; de Moraes Roso Mesquita, N.C.; de Paula Sousa, B.K.; Coimbra, L.D.; dos Santos, K.B.; Zorn, K.M.; Guido, R.V.; Ekins, S.; et al. Flavonoids from *Pterogyne nitens* as Zika virus NS2B-NS3 protease inhibitors. *Bioorg. Chem.* **2021**, *109*, 104719. [[CrossRef](#)]
79. Bhattacharya, K.; Bordoloi, R.; Chanu, N.R.; Kalita, R.; Sahariah, B.J.; Bhattacharjee, A. In silico discovery of 3 novel quercetin derivatives against papain-like protease, spike protein, and 3C-like protease of SARS-CoV-2. *J. Genet. Eng. Biotechnol.* **2022**, *20*, 43. [[CrossRef](#)]
80. Saakre, M.; Mathew, D.; Ravisankar, V. Perspectives on plant flavonoid quercetin-based drugs for novel SARS-CoV-2. *Beni-Suef Univ. J. Basic Appl. Sci.* **2021**, *10*, 21. [[CrossRef](#)]
81. Tang, Y.; Li, X.; Yuan, Y.; Zhang, H.; Zou, Y.; Xu, Z.; Xu, Q.; Song, J.; Deng, C.; Wang, Q. Network pharmacology-based predictions of active components and pharmacological mechanisms of *Artemisia annua* L. for the treatment of the novel Corona virus disease 2019 (COVID-19). *BMC Complement. Med. Ther.* **2022**, *22*, 56. [[CrossRef](#)]

82. Verma, S.; Pandey, A.K. Factual insights of the allosteric inhibition mechanism of SARS-CoV-2 main protease by quercetin: An in silico analysis. *3 Biotech* **2021**, *11*, 67. [[CrossRef](#)]
83. Arwa, P.S.; Zeraik, M.L.; Ximenes, V.F.; da Fonseca, L.M.; da Silva Bolzani, V.; Silva, D.H.S. Redox-active biflavonoids from *Garcinia brasiliensis* as inhibitors of neutrophil oxidative burst and human erythrocyte membrane damage. *J. Ethnopharmacol.* **2015**, *174*, 410–418. [[CrossRef](#)]
84. Chiang, C.H.; Yeh, C.Y.; Chung, J.G.; Chiang, I.T.; Hsu, F.T. Amentoflavone Induces Apoptosis and Reduces Expression of Anti-apoptotic and Metastasis-associated Proteins in Bladder Cancer. *Anticancer Res.* **2019**, *39*, 3641–3649. [[CrossRef](#)]
85. Funakoshi-Tago, M.; Okamoto, K.; Izumi, R.; Tago, K.; Yanagisawa, K.; Narukawa, Y.; Kiuchi, F.; Kasahara, T.; Tamura, H. Anti-inflammatory activity of flavonoids in Nepalese propolis is attributed to inhibition of the IL-33 signaling pathway. *Int. Immunopharmacol.* **2015**, *25*, 189–198. [[CrossRef](#)]
86. Salleh, W.M.N.H.W.; Abed, S.A.; Taher, M.; Kassim, H.; Tawang, A. The phytochemistry and biological diversity of *Ferulago* genus (Apiaceae): A systematic review. *J. Pharm. Pharmacol.* **2021**, *73*, 1–21. [[CrossRef](#)] [[PubMed](#)]
87. Zheng, X.; Liu, C.; Zhai, Y.; Li, L.; Wang, X.; Feng, W. Protection effect of amentoflavone in *Selaginella tamariscina* against TNF-alpha-induced vascular injury of endothelial cells. *Yao Xue Xue Bao = Acta Pharm. Sin.* **2013**, *48*, 1503–1509.
88. Jung, H.J.; Sung, W.S.; Yeo, S.H.; Kim, H.S.; Lee, I.S.; Woo, E.R.; Lee, D.G. Antifungal effect of amentoflavone derived from *Selaginella tamariscina*. *Arch. Pharm. Res.* **2006**, *29*, 746–751. [[CrossRef](#)] [[PubMed](#)]
89. Rizk, Y.S.; Santos-Pereira, S.; Gervazoni, L.; de Jesus Haridoim, D.; de Oliveira Cardoso, F.; da Silva Freitas de Souza, C.; Pelajo-Machado, M.; Carollo, C.A.; de Arruda, C.C.P.; Almeida-Amaral, E.E.; et al. Amentoflavone as an Ally in the Treatment of Cutaneous Leishmaniasis: Analysis of Its Antioxidant/Prooxidant Mechanisms. *Front. Cell. Infect. Microbiol.* **2021**, *11*, 615814. [[CrossRef](#)]
90. Rizk, Y.S.; Fischer, A.; de Castro Cunha, M.; Rodrigues, P.O.; Marques, M.C.S.; de Fátima Cepa Matos, M.; Kadri, M.C.T.; Carollo, C.A.; de Arruda, C.C.P. In vitro activity of the hydroethanolic extract and biflavonoids isolated from *Selaginella sellowii* on *Leishmania (Leishmania) amazonensis*. *Mem. Inst. Oswaldo Cruz* **2014**, *109*, 1050–1056. [[CrossRef](#)]
91. Lin, Y.M.; Flavin, M.T.; Schure, R.; Chen, F.C.; Sidwell, R.; Barnard, D.I.; Huffmann, J.H.; Kern, E.R. Antiviral Activities of Biflavonoids. *Planta Medica* **1999**, *65*, 120–125. [[CrossRef](#)]
92. Sun, C.M.; Yu, S.L.; Ou, J.C.; Syu, W.J. Test of the biflavones from *Selaginella moellendorffii* on the in vitro inhibition of HIV-1 protease. *J. Tradit. Chin. Med.* **1995**, *6*, 223–230.
93. Jayadevappa, M.K.; Karkera, P.R.; Siddappa, R.Y.; Telkar, S.; Karunakara, P. Investigation of plant flavonoids as potential dengue protease inhibitors. *J. Hermed Pharmacol.* **2020**, *9*, 366–373. [[CrossRef](#)]
94. Ghosh, R.; Chakraborty, A.; Biswas, A.; Chowdhuri, S. Computer aided identification of potential SARS CoV-2 main protease inhibitors from diterpenoids and biflavonoids of *Torreyia nucifera* leaves. *J. Biomol. Struct. Dyn.* **2020**, *40*, 2647–2662. [[CrossRef](#)]
95. Park, J.; Park, R.; Jang, M.; Park, Y.I.; Park, Y. Coronavirus enzyme inhibitors-experimentally proven natural compounds from plants. *J. Microbiol.* **2022**, *60*, 347–354. [[CrossRef](#)]
96. Saravanan, K.M.; Zhang, H.; Senthil, R.; Vijayakumar, K.K.; Sounderrajan, V.; Wei, Y.; Shakila, H. Structural basis for the inhibition of SARS-CoV2 main protease by Indian medicinal plant-derived antiviral compounds. *J. Biomol. Struct. Dyn.* **2020**, *40*, 1970–1978. [[CrossRef](#)]
97. Swargiary, A.; Mahmud, S.; Saleh, M.A. Screening of phytochemicals as potent inhibitor of 3-chymotrypsin and papain-like proteases of SARS-CoV2: An in silico approach to combat COVID-19. *J. Biomol. Struct. Dyn.* **2020**, *40*, 2067–2081. [[CrossRef](#)]
98. Lin, Y.M.; Zembower, D.E.; Flavin, M.T.; Schure, R.M.; Anderson, H.M.; Korba, B.E.; Chen, F.C. Robustaflavone, a naturally occurring biflavanoid, is a potent non-nucleoside inhibitor of hepatitis B virus replication in vitro. *Bioorg. Med. Chem. Lett.* **1997**, *7*, 2325–2328. [[CrossRef](#)]
99. Shivanika, C.; Deepak, C.S.; Ragunathan, V.; Tiwari, P.; Sumitha, A.; Brindha, D.V. Molecular docking, validation, dynamics simulations, and pharmacokinetic prediction of natural compounds against the SARS-CoV-2 main-protease. *J. Biomol. Struct. Dyn.* **2020**, *40*, 585–611. [[CrossRef](#)]
100. Menezes, J.C.; Campos, V.R. Natural biflavonoids as potential therapeutic agents against microbial diseases. *Sci. Total. Environ.* **2021**, *769*, 145168. [[CrossRef](#)]
101. Mondal, S.; Karmakar, A.; Mallick, T.; Begum, N.A. Exploring the efficacy of naturally occurring biflavone based antioxidants towards the inhibition of the SARS-CoV-2 spike glycoprotein mediated membrane fusion. *Virology* **2021**, *556*, 133–139. [[CrossRef](#)]
102. Ristovski, J.T.; Matin, M.M.; Kong, R.; Kusturica, M.P.; Zhang, H. In vitro testing and computational analysis of specific phytochemicals with antiviral activities considering their possible applications against COVID-19. *S. Afr. J. Bot.* **2022**, *151*, 248–258. [[CrossRef](#)]
103. Coluccia, A.; Puxeddu, M.; Nalli, M.; Wei, C.K.; Wu, Y.H.; Mastrangelo, E.; Elamin, T.; Tarantino, D.; Bugert, J.J.; Schreiner, B.; et al. Discovery of Zika Virus NS2B/NS3 Inhibitors That Prevent Mice from Life-Threatening Infection and Brain Damage. *ACS Med. Chem. Lett.* **2020**, *11*, 1869–1874. [[CrossRef](#)]
104. Scaturro, P.; Cortese, M.; Chatel-Chaix, L.; Fischl, W.; Bartenschlager, R. Dengue Virus Non-structural Protein 1 Modulates Infectious Particle Production via Interaction with the Structural Proteins. *PLoS Pathog.* **2015**, *11*, e1005277. [[CrossRef](#)]

105. Fassio, A.V.; Santos, L.H.; Silveira, S.A.; Ferreira, R.S.; de Melo-Minardi, R.C. nAPOLI: A graph-based strategy to detect and visualize conserved protein-ligand interactions in large-scale. *IEEE/ACM Trans. Comput. Biol. Bioinform.* **2019**, *17*, 1317–1328. [[CrossRef](#)]
106. Durrant, J.D.; McCammon, J.A. BINANA: A novel algorithm for ligand-binding characterization. *J. Mol. Graph. Model.* **2011**, *29*, 888–893. [[CrossRef](#)] [[PubMed](#)]

Disclaimer/Publisher’s Note: The statements, opinions and data contained in all publications are solely those of the individual author(s) and contributor(s) and not of MDPI and/or the editor(s). MDPI and/or the editor(s) disclaim responsibility for any injury to people or property resulting from any ideas, methods, instructions or products referred to in the content.